

See discussions, stats, and author profiles for this publication at: <https://www.researchgate.net/publication/249317477>

Engineered Biochar Reclaiming Phosphate from Aqueous Solutions: Mechanisms and Potential Application as a Slow-Release Fertilizer

ARTICLE in ENVIRONMENTAL SCIENCE & TECHNOLOGY · JULY 2013

Impact Factor: 5.33 · DOI: 10.1021/es4012977 · Source: PubMed

CITATIONS

34

READS

243

4 AUTHORS, INCLUDING:



Bin Gao

University of Florida

146 PUBLICATIONS 3,255 CITATIONS

[SEE PROFILE](#)



Jianjun Chen

University of Florida

131 PUBLICATIONS 1,718 CITATIONS

[SEE PROFILE](#)

Engineered Biochar Reclaiming Phosphate from Aqueous Solutions: Mechanisms and Potential Application as a Slow-Release Fertilizer

Ying Yao,^{†,‡} Bin Gao,^{*,†} Jianjun Chen,[§] and Liuyan Yang[†]

[†]Department of Agricultural and Biological Engineering, University of Florida, Gainesville, Florida 32611, United States

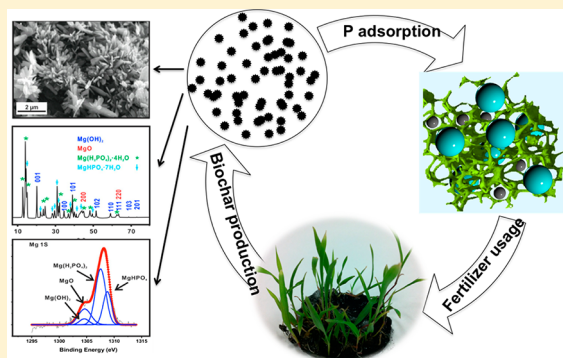
[‡]School of Chemical Engineering and the Environment, Beijing Institute of Technology, Beijing 100081, China

[§]Mid-Florida Research and Education Center, University of Florida, Apopka, Florida 32703, United States

[†]State Key Laboratory of Pollution Control and Resource Reuse, School of the Environment, Nanjing University, Nanjing 210046, China

Supporting Information

ABSTRACT: This work explored the potential application of an engineered biochar prepared from Mg-enriched tomato tissues to reclaim and reuse phosphate (P) from aqueous solution. Findings from batch sorption experiments suggested that, although sorption of P on the biochar was controlled by relatively slow kinetics, the maximum P sorption capacity of the biochar could reach $>100 \text{ mg}\cdot\text{g}^{-1}$. Mathematical modeling and postsorption characterization results indicated that the sorption was mainly controlled by two mechanisms: precipitation of P through chemical reaction with Mg particles and surface deposition of P on Mg crystals on biochar surfaces. Most of the P retained in the engineered biochar was bioavailable and could be released equally at multiple successive extractions. In addition, the P-laden biochar significantly stimulated grass seed germination and growth. These results suggested the postsorption biochar can be cycled back directly to soils as an effective slow-release P-fertilizer.



INTRODUCTION

Phosphorus is a limiting nutrient for the growth of organisms and plants and is an indicator of surface water quality.¹ Excessive phosphorus from both point and nonpoint sources into natural waters is known to cause eutrophication which is occurring throughout the world.^{2–5} Dissolved phosphate of $\sim 0.02 \text{ mg}\cdot\text{L}^{-1}$ is considered to have potential that leads to profuse algal growth in waters.⁶ Accelerated eutrophication not only affects the aquatic ecosystems but also indirectly hinders the economic progress. The combined costs were approximately \$2.2 billion annually as a result of eutrophication in U.S. freshwaters.⁷ It is therefore very important to develop effective technologies to remove phosphate from aqueous solutions prior to their discharge into runoff and natural water bodies.

The role of biochar (pyrogenic black carbon derived from incomplete biomass combustion) in political and academic communities has received much attention in recent years. Biochar is widely recognized as an important cost-effective adsorbent storing chemical contaminants including heavy metals, organic compounds, and other environmental pollutants.^{8–12} The use of carbon/biochar to remove phosphate from aqueous solutions is an emerging and promising concept with plenty of advantages over traditional wastewater treatment technologies, such as lower cost and/or being more environment-

mentally friendly.¹³ Most of the traditional engineered carbons (e.g., activated carbon and biochar), however, have limited ability to adsorb P or other anionic nutrients. For example, Namasivayam et al.¹⁴ and Bhargava et al.¹⁵ reported that the P adsorption capacity of activated carbons derived from coir pith and tamarind nut shell was only about $5.1 \text{ mg}\cdot\text{g}^{-1}$ and $5.0 \text{ mg}\cdot\text{g}^{-1}$, respectively. Yao et al.¹⁶ tested thirteen biochars made from different biomass feedstocks and found most of them had little/no ability to sorb phosphate from aqueous solutions. Chen et al.¹⁷ reported that magnetic biochars made from iron-treated orange peel powders had a P adsorption capacity of only around $1.2 \text{ mg}\cdot\text{g}^{-1}$.

In order to improve the sorption ability of biochars to aqueous P, several investigations have been conducted to synthesize engineer biochars with novel structures and surface properties.^{13,17–22} In particular, it has been reported that engineered Mg–biochar nanocomposites with nanosized magnesium oxides (MgO) attached on carbon surfaces within the biochar matrix have superior sorption ability to aqueous P.^{13,18,20} For example, the MgO–biochar nanocomposites

Received: March 24, 2013

Revised: July 10, 2013

Accepted: July 13, 2013

Published: July 13, 2013

synthesized through pyrolyzing anaerobically digested sugar beet tailings¹³ or MgCl₂-pretreated agricultural residues²⁰ both showed an extremely high sorption capacity to P (>100 mg·g⁻¹), which is much higher than that of many carbon-based and other commercial adsorbents reported in the literature (<20 mg·g⁻¹).^{5,23–29} The superior P sorption ability of these MgO–biochar nanocomposites is attributed to the presence of the nanosized MgO particles on the biochar surfaces, which can serve as active adsorption sites for aqueous P.^{13,20} Because the production of the MgO–biochar nanocomposites involves either chemical or microbial pretreatment procedures, an innovative approach was recently developed to synthesize a new P-removal engineered biochar by direct pyrolysis of plant biomass residues enriched with Mg element through bioaccumulation.¹⁹ The new engineered biochar has nanosized Mg(OH)₂ and MgO particles on its surfaces and showed promising potential to adsorb P from aqueous solutions.¹⁹ However, the sorption characteristics and mechanisms of P on this engineered biochar prepared from Mg-enriched plant tissues have not been examined previously.

Previous studies of the P-removal biochars also have proposed that the postsorption biochars could potentially be applied directly to cropland as a fertilizer because the spent biochars may contain a high amount of P. For example, the P contents in the postsorption MgO–biochar nanocomposites derived from anaerobically digested sugar beet tailings and MgCl₂-treated biomass were all greater than 10%, comparable to or even greater than that of commercial phosphorus fertilizers. In addition to P-fertilizer supply, the P-laden biochars, when applied to soils, would also be a carbon sink because of their relatively high recalcitrance or resistance to abiotic and biotic degradation.^{30–35} Nevertheless, the bioavailability of the adsorbed P in the spent engineered biochars is still unknown. To the authors' best knowledge, no investigations have been conducted previously to determine desorption mechanisms, release characteristics, or biological effects of adsorbed P in spent engineered biochars.

The overarching objective of this study was to determine whether engineered biochars can be used to reclaim aqueous P and then be applied to soils as a P-fertilizer. A series of laboratory experiments were conducted to determine the mechanisms and characteristics of P adsorption on an engineered biochar prepared from Mg-enriched tomato tissues. The bioavailability, desorption characteristics, and seed germination ability of the adsorbed P within the spent (i.e., P-laden) biochar were also evaluated. The specific objectives were as follows: (1) measure the sorption characteristics of P to the engineered biochar, (2) characterize the postsorption biochar to identify the governing P sorption/desorption mechanisms, (3) measure the release characteristics of P from the postsorption biochar, and (4) determine the biological effects of the postsorption biochar on seed germination and seedling growth.

MATERIALS AND METHODS

Materials. The engineered biochar used in this study is a Mg–biochar nanocomposite prepared by pyrolyzing Mg-enriched tomato leaves inside a furnace under a N₂ environment at 600 °C. After washing with deionized (DI) water to remove impurities (mainly residual ashes), the biochar was oven-dried (80 °C) and sealed in a container prior to use. More information about the preparation and characterization of the engineered biochar can be found in Yao et al.¹⁹ Phosphate

solutions were prepared by dissolving potassium phosphate monobasic (KH₂PO₄) in DI water. All the chemicals used in the study are A.C.S certified and from Fisher Scientific.

P Adsorption. Adsorption kinetics of phosphate on the biochar were examined by mixing 0.1 g of the sorbent with 50 mL of 30.6 mg·L⁻¹ (i.e., 0.3 mM) phosphate solutions in 68 mL digestion vessels (Environmental Express) at room temperature (22 ± 0.5 °C). The vessels were then shaken at 55 rpm in a mechanical shaker. At appropriate time intervals, the vessels were withdrawn and the mixtures were immediately filtered through 0.22 μm pore size nylon membrane filters (GE cellulose nylon membrane).

Adsorption isotherm of phosphate on the biochar was determined similarly by mixing 0.1 g of biochar with 50 mL of phosphate solutions of different concentrations ranging from 3.1 to 588.1 mg·L⁻¹ in the digestion vessels. The vessels were shaken in the mechanical shaker for 24 h at room temperature (sufficient to reach adsorption equilibrium). The samples were then withdrawn and filtered to determine adsorbed phosphate concentrations. In addition, pH values of solutions before and after phosphate sorption were measured with a pH meter (Fisher Scientific Accumet Basic AB15). Phosphate concentrations on the solid phase were calculated on the basis of the initial and final aqueous concentrations, which were determined by inductively coupled plasma atomic emission spectroscopy (ICP-AES). The postadsorption biochar samples were collected, rinsed with deionized water, and dried at 80 °C for further experiments.

Effects of competing compounds on phosphate sorption by the biochar were investigated by adding common coexisting anions (chloride, nitrate, or bicarbonate) or organic matter (humic acid (HA)) to the 30.6 mg·L⁻¹ (0.3 mM/L) phosphate solutions into separate digestion vessels. On the basis of their typical concentrations in wastewater,^{36–41} 50.0 mg·L⁻¹ Cl⁻ (NaCl, 1.4 mM·L⁻¹), 15.0 mg N·L⁻¹ NO₃⁻ (NaNO₃, 0.24 mM·L⁻¹), 80.0 mg·L⁻¹ HCO₃⁻ (NaHCO₃, 1.3 mM·L⁻¹), 2.0 mg·L⁻¹ humic acid (HA), or their mixture was used in this work. The ratio of adsorbent to initial P solution was the same as the kinetics/isotherm experiment. The vessels were shaken in the mechanical shaker for 24 h at room temperature. The same procedures were used to determine aqueous and adsorbed phosphate concentrations.

All the adsorption experiments were conducted in duplicate, and the average experimental data are reported. Additional measurements were obtained when the duplicates had a difference larger than 5%.

Postsorption Characterization. The physicochemical properties of the engineered biochar have been measured previously and detailed information can be found in Yao et al.¹⁹ In this work, the characterization experiments thus were only conducted for the postsorption biochar samples. Scanning electron microscope (SEM) imaging analysis was conducted using a JEOL JSM-6400 scanning microscope. Varying magnifications were used to examine the structure and surface characteristics of the postsorption engineered biochar. Surface element analysis was also conducted simultaneously with the SEM at the same surface locations using energy dispersive X-ray spectroscopy (EDX, Oxford Instruments Link ISIS). The EDX can provide rapid qualitative or, with adequate standards, semiquantitative analysis of elemental composition with a sampling depth of 1–2 μm.⁴² X-ray diffraction (XRD) analysis was carried out to identify any crystallographic structure in the postsorption biochar using a computer-controlled X-ray

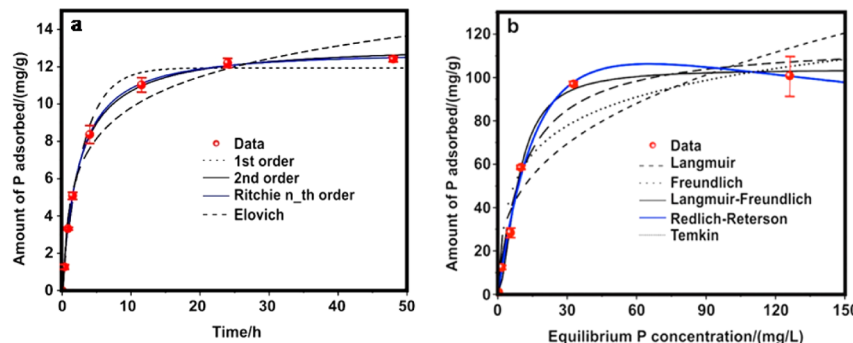


Figure 1. Adsorption kinetic (a) and isotherm (b) data and modeling for phosphate on the engineered biochar. Symbols are experimental data, and lines are model results.

Table 1. Best-Fit Parameter Values from Model Simulations of P Adsorption Kinetics, Isotherms, and Desorption Kinetics^a

	parameter 1	parameter 2	parameter 3	R ²
Adsorption Kinetics				
first-order	$k_1 = 0.337 \pm 0.084 \text{ (h}^{-1}\text{)}$	$q_e = 11.950 \pm 0.800 \text{ (mg}\cdot\text{g}^{-1}\text{)}$		0.989
second-order	$k_2 = 0.032 \pm 0.004 \text{ (g}\cdot\text{mg}^{-1}\cdot\text{h}^{-1}\text{)}$	$q_e = 13.260 \pm 0.33 \text{ (mg}\cdot\text{g}^{-1}\text{)}$		0.999
<i>n</i> _th-order	$k_n = 0.406 \pm 0.038 \text{ (g}^{n-1}\cdot\text{mg}^{1-n}\text{h}^{-1}\text{)}$	$q_e = 12.820 \pm 0.57 \text{ (mg}\cdot\text{g}^{-1}\text{)}$	$n = 1.744 \pm 0.318$	1.000
Elovich	$\beta = 2.390 \pm 0.439 \text{ (g}\cdot\text{mg}^{-1}\text{)}$	$\alpha = 2.538 \pm 0.851 \text{ (mg}\cdot\text{g}^{-1}\cdot\text{h}^{-1}\text{)}$		0.975
Adsorption Isotherms				
Langmuir	$K = 0.090 \pm 0.067 \text{ (L}\cdot\text{mg}^{-1}\text{)}$	$Q = 116.600 \pm 26.590 \text{ (mg}\cdot\text{g}^{-1}\text{)}$		0.972
Freundlich	$K_f = 21.690 \pm 23.400 \text{ (mg}^{(1-n)}\text{ L}^n\cdot\text{g}^{-1}\text{)}$	$n = 0.342 \pm 0.263$		0.850
Langmuir-Freundlich	$K_{lf} = 0.023 \pm 0.054 \text{ (L}^n\cdot\text{mg}^{-n}\text{)}$	$Q = 103.800 \pm 17.36 \text{ (mg}\cdot\text{g}^{-1}\text{)}$	$n = 1.749 \pm 1.219$	0.991
Redlich-Peterson	$K_r = 0.015 \pm 0.028 \text{ (L}^n\cdot\text{mg}^{-n}\text{)}$	$a = 7.082 \pm 2.866 \text{ (L}^n\cdot\text{mg}^{-n}\text{)}$	$n = 1.298 \pm 0.326$	0.994
Temkin	$b = 129.700 \pm 55.900 \text{ (J}\cdot\text{g}\cdot\text{mg}^{-1}\text{)}$	$A = 2.008 \pm 2.832 \text{ (L}\cdot\text{mg}^{-1}\text{)}$		0.912
Desorption Kinetics				
second-order	$k_{ds} = 0.126 \pm 0.122 \text{ (L}\cdot\text{mg}^{-1}\cdot\text{h}^{-1}\text{)}$	$C_e = 11.740 \pm 1.490 \text{ (mg}\cdot\text{L}^{-1}\text{)}$		0.916

^aConfidence level (CL) = 95%.

diffractometer (Philips Electronic Instruments) equipped with a stepping motor and graphite crystal monochromator. Crystalline compounds in the samples were identified by comparing diffraction data against a database compiled by the Joint Committee on Powder Diffraction and Standards. In addition, X-ray photoelectron spectroscopy (XPS) measurements were carried out with a PHI 5100 series ESCA spectrometer (PerkinElmer) to determine the elemental composition on the sample surface.

P Release. A bioavailable phosphorus test was carried out using the Mehlich 3 soil test method.⁴³ P was extracted at a spent biochar: extractant volumetric ratio of 1:10. Mehlich 3 extractant consists of 0.2 M CH₃COOH, 0.25 M NH₄NO₃, 0.015 M NH₄F, 0.013 M HNO₃, and 0.001 M EDTA. The final pH of the extracting solution was about 2.5 ± 0.1. The samples were shaken at 200 rpm for 5 min at room temperature (22 ± 0.5 °C) and then filtered through Whatman No. 42 filter paper to determine the extractable P concentrations. The extraction experiment was replicated three times, and the average data and standard deviations are reported.

Kinetics of phosphorus release from the postsorption biochar into DI water was measured by mixing 0.3 g of the sample with 120 mL of DI water at room temperature (22 ± 0.5 °C). The contents of P in the aqueous solution were then determined after 1, 2, 3, 6, 10, 24, 48, 120, and 144 h. For the next 11 days, the biochar sample was filtered out from the solution and added to 120 mL of fresh DI water every day to release P. The kinetics and release experiments were replicated three times, and the average data and standard deviations are reported.

Seeds Germination and Early Stage Seedling Growth Bioassay.

The seeds germination assay was carried out by spreading the same number of grass seeds (Brown Top Millet) on a layer of filter paper moistened with DI water in containers with or without 0.1 g of P-laden biochar with ≥4 replicates. All replicates were incubated at room temperature, and successfully emerged seeds (those with shoots longer than 0.5 cm) were counted once significant germination was observed. The early stage (first 13 days) seedling growth was also determined, and 10 seedlings from each group were randomly collected for statistical analysis.

Statistics. The coefficient of determination (R^2), *p*-value, standard deviation, and other statistics were analyzed by OriginPro 8.5. Matlab Toolbox was used to fit all kinetics and isotherm data, and the standard errors of the fitted coefficients were with 95% confidence interval. Differences between the numbers of seeds germination were statistically analyzed with the *t* test and one-way ANOVA with a significance level of 0.05 (*p* < 0.05). Error bars were used to represent standard deviations of multiple determinations.

RESULTS AND DISCUSSION

Adsorption Kinetics and Isotherms. Kinetics study indicated that the sorption of P on the engineered biochar increased smoothly over time and reached equilibrium at around 24 h (Figure 1a). This result is similar to the sorption kinetics of P on the MgO–biochar nanocomposites produced from digested sugar beet tailings, although the biochar used in this study contained both MgO and Mg(OH)₂ particles.^{13,19} Different mathematical models were applied in this study to

describe the adsorption kinetics of P on the biochar. In addition to the commonly used pseudofirst-order and pseudosecond-order models, the Ritchie *n*_th-order model and the Elovich model were also used and the governing equations are¹³

$$\frac{dq_t}{dt} = k_1(q_e - q_t) \quad \text{first-order} \quad (1.1)$$

$$\frac{dq_t}{dt} = k_2(q_e - q_t)^2 \quad \text{second-order} \quad (1.2)$$

$$\frac{dq_t}{dt} = k_n(q_e - q_t)^n \quad \text{Richie } n\text{-th-order} \quad (1.3)$$

$$\frac{dq_t}{dt} = \alpha \exp(-\beta q_t) \quad \text{Elovich} \quad (1.4)$$

where q_t ($\text{mg}\cdot\text{g}^{-1}$) and q_e ($\text{mg}\cdot\text{g}^{-1}$) are the amount of P adsorbed at time t and at equilibrium, respectively, k_1 (h^{-1}), k_2 ($\text{g}\cdot\text{mg}^{-1}\cdot\text{h}^{-1}$), and k_n ($\text{g}^{n-1}\cdot\text{mg}^{1-n}\cdot\text{h}^{-1}$) are the first-order, second-order, and *n*_th-order adsorption rate constants, α ($\text{mg}\cdot\text{g}^{-1}\cdot\text{h}^{-1}$) is the initial adsorption rate, and β ($\text{g}\cdot\text{mg}^{-1}$) is the desorption constant. The first-order, second-order, and *n*_th-order models describe the kinetics of the solid-solution system based on mononuclear, binuclear, and *n*-nuclear adsorption, respectively, with respect to the sorbent capacity, and the Elovich model is an empirical equation considering the contribution of desorption.¹³

The best-fit parameters of the kinetics models are listed in Table 1. All these models closely reproduced the kinetic data (Figure 1a) with R^2 exceeding 0.97. The *n*_th-order ($n = 1.74$) models fitted the data slightly better than other models with a R^2 of 1.00, suggesting that the adsorption of P on the engineered biochar could be controlled by multiple mechanisms. Previous studies showed that intraparticle diffusion processes could play an important role in controlling the sorption of contaminants on carbon materials.^{44,45} In this study, the sorption kinetics of P on the engineered biochar might also be affected by the intraparticle diffusion mechanism because the pre-equilibrium P adsorption data showed a linear dependency ($R^2 = 0.891$) on the square root of time (Figure S1, Supporting Information).

The maximum P sorption capacity of the engineered biochar obtained from the isotherm study was greater than 100 $\text{mg}\cdot\text{g}^{-1}$ (Figure 1b), indicating the biochar could be used as an effective sorbent to remove P from aqueous solutions. In addition, this high sorption capacity also suggests that the spent engineered biochar, which was laden with more than 10% of P, could potentially be used as a P-fertilizer. Five commonly used isotherm equations were used to simulate the experimental isotherms, and the governing equations are^{13,46}

$$q_e = \frac{KQC_e}{1 + KC_e} \quad \text{Langmuir} \quad (2.1)$$

$$q_e = K_f C_e^n \quad \text{Freundlich} \quad (2.2)$$

$$q_e = \frac{K_{lf}QC_e^n}{1 + K_{lf}C_e^n} \quad \text{Langmuir-Freundlich} \quad (2.3)$$

$$q_e = \frac{K_r C_e}{1 + a C_e} \quad \text{Redlich-Peterson} \quad (2.4)$$

$$q_e = \frac{RT}{b} \ln(AC_e) \quad \text{Temkin} \quad (2.5)$$

where K ($\text{L}\cdot\text{mg}^{-1}$), K_f ($\text{mg}^{(1-n)}\cdot\text{L}^n\cdot\text{g}^{-1}$), K_{lf} ($\text{L}^n\cdot\text{mg}^{-n}$), and K_r ($\text{L}\cdot\text{g}^{-1}$) represent the Langmuir bonding term related to interaction energies, the Freundlich affinity coefficient, Langmuir-Freundlich affinity parameter, and the Redlich-Peterson isotherm constants, respectively, Q ($\text{mg}\cdot\text{g}^{-1}$) denotes the Langmuir maximum capacity, C_e ($\text{mg}\cdot\text{L}^{-1}$) is the equilibrium solution concentration of the sorbate, n (dimensionless) is the Freundlich linearity constant, a ($\text{L}^n\cdot\text{mg}^{-n}$) is the Redlich-Peterson isotherm constant, and b ($\text{J}\cdot\text{g}\cdot\text{mg}^{-1}$) and A ($\text{L}\cdot\text{mg}^{-1}$) are the Temkin isotherm constants.^{13,46} The Langmuir model assumes monolayer adsorption onto a homogeneous surface with no interactions between the adsorbed molecules, while the other models are empirical or semiempirical equations, which are often used to describe heterogeneous sorption processes.

Almost all the isotherm models reproduced the adsorption data well, except the Freundlich equation (Figure 1b). The best-fit model parameters are also listed in Table 1. Fittings of the Langmuir-Freundlich and Redlich-Peterson ($R^2 = 0.994$) matched the experimental data better than other models, suggesting that the interaction between P and the biochar could be affected by both the Langmuir and the Freundlich processes. This result is consistent with the kinetics study results that the sorption of P on the engineered biochar could be governed by multiple mechanisms.

Adsorption/Desorption Mechanisms. In previous studies of P sorption on MgO-biochar nanocomposites prepared from anaerobically digested biomass, the interaction was mainly attributed to the surface deposition mechanism between P ions and the MgO particles on carbon surfaces within the matrix.¹³ Because surfaces of the engineered biochar used in this study were dominated by both Mg(OH)₂ and MgO particles,¹⁹ the P sorption mechanism could be different from previous studies. In this study, the XRD spectra of the postsorption biochar (i.e., P-laden biochar) showed strong signals of not only the pre-existing Mg oxyhydroxides but also new Mg-P crystals in the forms of MgHPO₄ and Mg(H₂PO₄)₂ with calculated particle sizes of 30.3 and 32.4 nm, respectively (Figure 2). The XRD

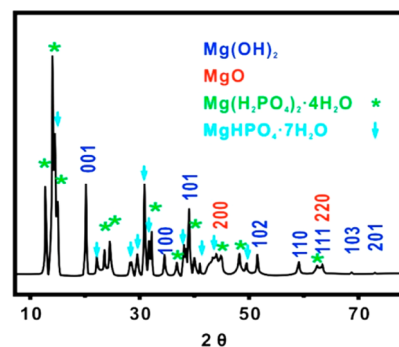


Figure 2. XRD spectrum of P-laden biochar.

results suggested that, in addition to surface deposition mechanism as reported previously, precipitation of P by Mg released from the engineered biochar could also play an important role in the P removal from aqueous solutions. The SEM-EDX analysis confirmed the formation of the new Mg-P crystals within the biochar matrix (Figure 3). As shown in the SEM image, the postsorption biochar showed clusters of

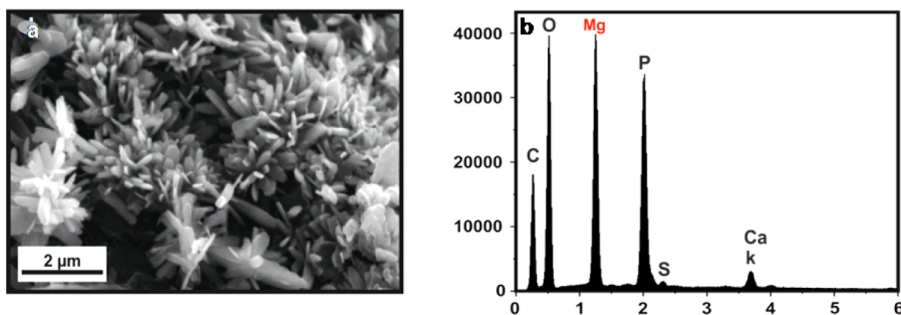


Figure 3. SEM image and EDX spectrum of P-laden biochar morphological structures.

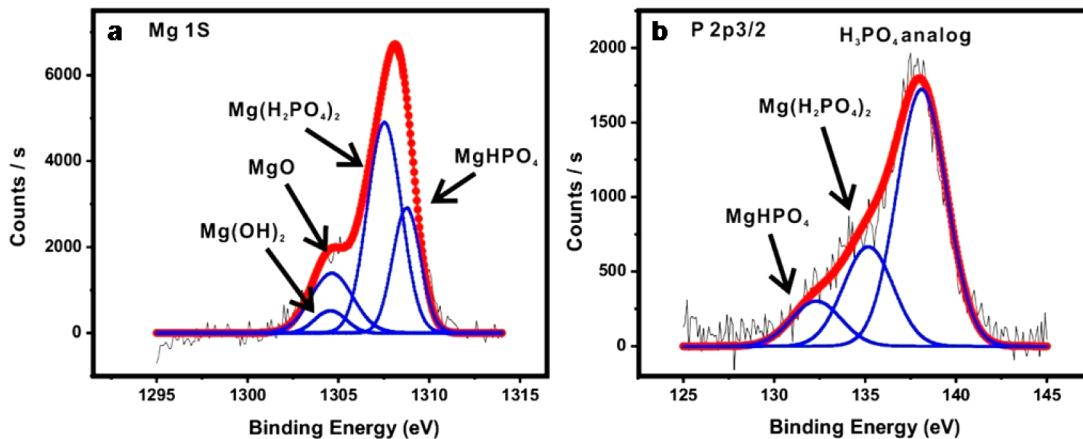


Figure 4. XPS spectra of the Mg 1s (a) and P 2p3/2 (b) region for P-laden biochar.

nanosized Mg–P flakes on the carbon surface, which were not observed in the original biochar samples as reported in Yao et al.¹⁹ The measurements of the solution pH before and after the sorption indicated that the initial and final pH of all the solutions was around 5.2 and 7.9, respectively, which is consistent with the precipitation mechanism. At this pH range, phosphate in the solution exists in the species of HPO_4^{2-} and HPO_4^- , which would precipitate the released Mg to form the MgHPO_4 and $\text{Mg}(\text{H}_2\text{PO}_4)_2$ crystals.

The precipitation of P on the biochar was further confirmed by XPS analysis (Figure 4). The Mg 1s spectrum (Figure 4a) clearly demonstrates the presence of four compounds on the P-laden biochar surface.⁴⁷ The molar percentage of Mg oxyhydroxides, MgHPO_4 , and $\text{Mg}(\text{H}_2\text{PO}_4)_2$ on the biochar surface were around 21.9%, 25.8%, and 52.3%, respectively. The Mg oxyhydroxides on the carbon surface decreased dramatically after the sorption, because they reacted with the P ions to form the Mg–P precipitates. Although both MgO and $\text{Mg}(\text{OH})_2$ have low solubility, the presence of P anions in the solution may facilitate their dissolution to form more insolubility of P salt, such as $\text{Mg}(\text{H}_2\text{PO}_4)_2$ and MgHPO_4 . The newly formed P salts prefer to nucleate and grow on the carbon surface within the biochar because of lower surface energy,⁴⁸ which often can be confirmed by examining morphology and crystallization of the salt particles. In this study, the nanoplatelet particles on the original biochar surface,¹⁹ which is a common structural morphology of Mg hydroxide, were converted into nanorods growing in bunches after the P sorption experiment.^{49,50} The significant altering in morphology of nanoparticles before and after P sorption suggests that precipitation played an important role in P removal by the engineered biochar produced from Mg-enriched plant tissues.

It is interesting to draw attention to the XPS spectrum of P 2p3/2 on the surface of the P-laden biochar (Figure 4b). The binding energies of the P 2p3/2 peak represent three compounds. The binding energy at 132.3 eV corresponds to MgHPO_4 (11.2%), while that at 135.2 eV corresponds to $\text{Mg}(\text{H}_2\text{PO}_4)_2$ (24.8%).^{51,52} The molar ratio between MgHPO_4 and $\text{Mg}(\text{H}_2\text{PO}_4)_2$ is 0.45, which is similar to that of the XPS analysis of Mg 1s (0.49). The most intense component at a high binding energy of 138.16 eV is associated with the presence of P analog (64.0%) in which there is no reaction between P anions and metallic cations. Therefore, the extremely high content of PO₄ analog can be attributed to the surface deposition mechanisms. In addition to the interaction between P and MgO particles as reported in our previous studies, the other three Mg salts including the two precipitates (i.e., $\text{Mg}(\text{OH})_2$, MgHPO_4 , and $\text{Mg}(\text{H}_2\text{PO}_4)_2$ particles) can also adsorb additional P analog by hydrogen bonding.^{53–55} The number of the additional P overlayers should be around two layers presumed from the fitting XPS spectrum of P 2p3/2. Findings from the XPS analysis of P 2p3/2 on postsorption biochar indicated that, in addition to precipitation, surface deposition could also play an important role in controlling the adsorption of P on the engineered biochar.

Findings from the experiment with competing compounds further showed the important role of the surface deposition mechanism in controlling phosphate sorption on the biochar. While the HA showed no obvious effect, the presence of each of the anions and their mixture reduced the sorption of phosphate on the biochar to about 5–40% (Figure 5). The reduction of phosphate sorption could be attributed to the completion or blocking of the surface adsorption sites by the

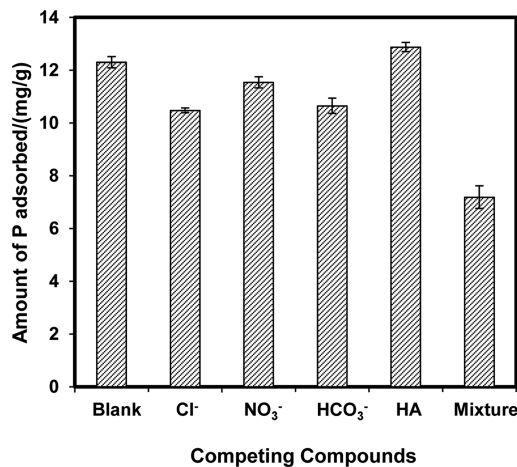


Figure 5. Effects of competing compounds on phosphate sorption on the engineered biochar.

coexisting anions (anions like Cl^- and NO_3^- could not precipitate Mg^{2+}). Although the coexisting anions have negative effects, the experimental results showed that the engineered biochar prepared in this work is still very effective in reclaiming phosphate from wastewater, particularly under low anion concentration conditions.

In summary, findings from the sorption experiments and postsorption characterizations indicated that the removal of P by the engineered biochar from Mg-enriched tomato tissues is mainly controlled by both the precipitation (strong chemical bond) and surface deposition (weak chemical bond) mechanisms (Figure 6). Because the majority of the P (64%) in postsorption biochar is deposited on the Mg surface with the carbon matrix through weak chemical bonds (hydrogen bonding), it may be bioavailable through desorption processes (Figure 6), when the exhausted biochar is applied to soils as amendment. Moreover, the potential release of Mg from the biochar could improve Mg supply in the amended soils (especially under acidic conditions) to benefit crop growth. Hence, the spent biochar may have the potential to serve as a P-fertilizer and improve soil fertility.

P Desorption from P-Laden Biochar as a Slow-Release Fertilizer. To assess the bioavailability of P, the extractable P content of the postsorption (P-laden) biochar was determined with the Mehlich 3 method, which is the widely accepted laboratory index of plant-available P in soil. Results showed that the extractable P of the exhausted biochar was around $7555.5 \pm 10.5 \text{ mg P kg}^{-1}$, much higher than that of optimum P in soil for plant growth and crop yields, i.e., $45\text{--}50 \text{ mg P kg}^{-1}$.⁵⁶ About 19% of total P in postsorption biochar was Mehlich3 extractable which is consistent with findings of published studies.⁵⁷ This result suggests a high feasibility of using the engineered biochar to treat and reclaim P from wastewater and then apply the P-laden biochar directly to soil as a fertilizer for eco-friendly and sustainable production of crops.

Desorption kinetics study of the P-laden biochar showed the slow release of the P, and the equilibrium was reached after 30 h (Figure 7a). On the basis of the adsorption/desorption mechanisms (Figure 6), two layers of P are adsorbed on the biochar through weak chemical bonds (e.g., hydrogen and electrostatic bonds). Thus, desorption of the P in the two layers from the biochar can be described by the second-order kinetics:

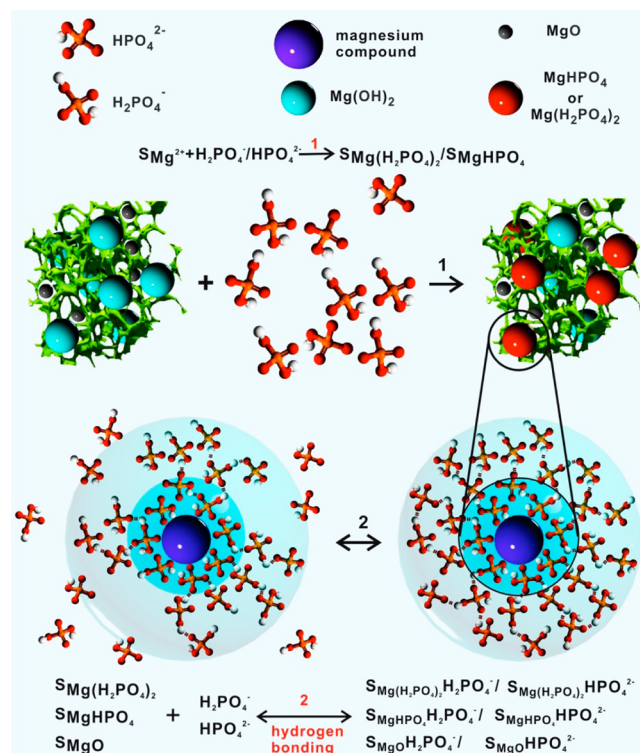


Figure 6. Illustration scheme of adsorption and desorption mechanisms of P on the engineered biochar surface (S). The green colored structures represent biochar matrix, and the purple colored magnesium compound represents MgO , MgOH , MgHPO_4 , or $\text{Mg}(\text{H}_2\text{HPO}_4)_2$. Drawing is not to scale.

$$\frac{dC_t}{dt} = k_{ds}(C_e - C_t)^2 \quad (3)$$

where k_{ds} is the second-order rate constant ($\text{L mg}^{-1} \text{ h}^{-1}$). The equation was then solved with a zero initial condition for C_t :

$$C_t = \frac{C_e^2 k_{ds} t}{C_e k_{ds} t + 1} \quad (4)$$

Simulations from the eq 4 matched the experimental data well with $R^2 = 0.916$ (Table 1), which is consistent with the surface adsorption–desorption mechanism as discussed previously. Because of the strong sorption of P on the Mg surface, only a small amount of P was released into the solution at equilibrium. As shown in Figure 7b, however, this release was repeatable when fresh solution was introduced to the system (to mimic conditions under plant growth, which depletes released P). During the 11 successive slow releasing experiments, about the same amount of P (3.2% of total adsorbed P) was released at each run, indicating the exhausted biochar could be used as a slow-P-release fertilizer when applied to soils. In addition, the TGA analysis showed that the P-laden biochar has similar thermal stability to that of the original sample (Figure S2, Supporting Information), suggesting that, in addition to be a P-fertilizer, the post-sorption biochar could also be used as a carbon sequester.

Seeds Germination and Early Stage Seedling Growth Bioassay. Bioassay of seeds germination and early stage seedlings growth is a simple and commonly used ecotoxicological test for evaluating the impact of biochar amendment on crop growth.⁵⁸ The assay results in this work showed that the

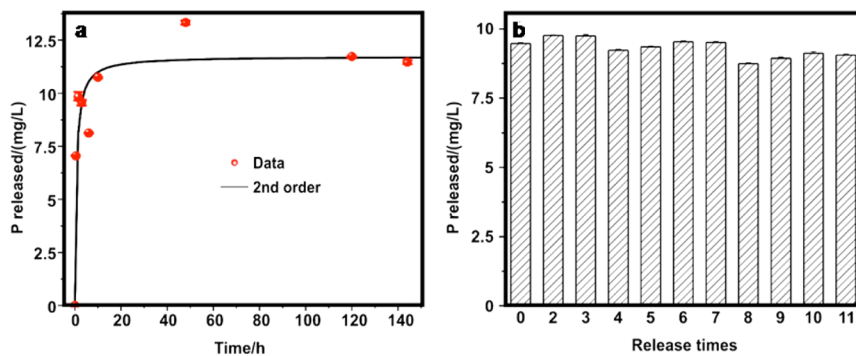


Figure 7. (a) Desorption kinetics, symbols are experimental data and the line is model results. (b) Successive and repeatable release of phosphate by P-laden biochar as each time fresh solution was introduced to the system to mimic conditions under plant growth.

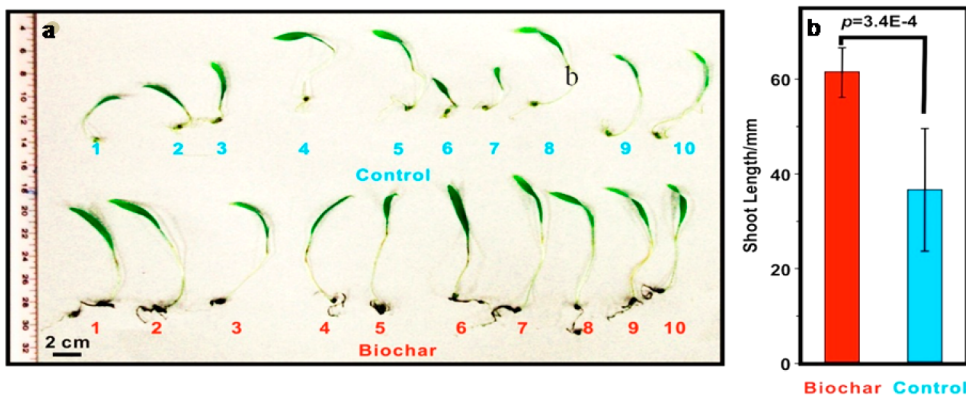


Figure 8. Comparison of grass seedlings between P-laden biochar and control groups.

P-laden biochar nanocomposite could promote seed germination. The addition of the biochar increased seed germination rate from 53% to 85%, and the results are statistically significant ($p < 0.001$). After a 13-day growth, the length of the grasses with biochar addition was much longer than that in control groups (Figure 8). Furthermore, leaves of the grasses from the biochar groups were greener and stronger. These results were consistent with findings in the literature that a sufficient supply of phosphorus may not only increase the germination rate but also promote the radicle growth.⁵⁹ The assay results further confirmed that the postsorption, P-laden engineered biochar could be used as a slow-release fertilizer to be applied to soils to improve soil quality and productivity.

Environmental Implications. The engineered biochar converted from Mg-enriched tomato tissues showed strong P removal ability. The spent biochar, which is P laden, behaved as a slow-release fertilizer and could release P into aqueous solution multiple times (mimics slow release P source for plant uptake) to stimulate grass seeds' emergence and growth. The concept and findings from this study can be used to develop new sustainable and eco-friendly strategies to synthesize and apply the engineered biochar to reclaim P, reduce eutrophication, fertilize soils, improve soil quality, and sequester carbon.

ASSOCIATED CONTENT

Supporting Information

Relation between P adsorbed and square root of time before equilibrium; TGA curves of original and P-laden biochars. This material is available free of charge via the Internet at <http://pubs.acs.org>.

AUTHOR INFORMATION

Corresponding Author

*E-mail: bg55@ufl.edu; phone: (352) 392-1864 ext. 285.

Notes

The authors declare no competing financial interest.

ACKNOWLEDGMENTS

This research was partially supported by the NSF through grants: CBET-1054405 and CHE-1213333.

REFERENCES

- (1) Almeelbi, T.; Bezbarua, A. Aqueous phosphate removal using nanoscale zero-valent iron. *J. Nanopart. Res.* **2012**, *14*, 1–14.
- (2) Smith, V. H. Eutrophication of freshwater and coastal marine ecosystems - A global problem. *Environ. Sci. Pollut. Res.* **2003**, *10*, 126–139.
- (3) Penn, C. J.; Warren, J. G. Investigating phosphorus sorption onto kaolinite using isothermal titration calorimetry. *Soil Sci. Soc. Am. J.* **2009**, *73*, 560–568.
- (4) Bhargava, D. S.; Sheldarkar, S. B. Use of Tnsac in phosphate adsorption studies and relationships - Literature, experimental methodology, justification and effects of process variables. *Water Res.* **1993**, *27*, 303–312.
- (5) Ozacar, M. Adsorption of phosphate from aqueous solution onto alunite. *Chemosphere* **2003**, *51*, 321–327.
- (6) USEPA *Ecological restoration: A tool to manage stream quality*, Report EPA 841-F-95-007; US EPA: Washington, DC, USA, 1995.
- (7) Dodds, W. K.; Bouska, W. W.; Eitzmann, J. L.; Pilger, T. J.; Pitts, K. L.; Riley, A. J.; Schloesser, J. T.; Thornbrugh, D. J. Eutrophication of US freshwaters: Analysis of potential economic damages. *Environ. Sci. Technol.* **2008**, *43*, 12–19.

- (8) Kasozi, G. N.; Zimmerman, A. R.; Nkedi-Kizza, P.; Gao, B. Catechol and humic acid sorption onto a range of laboratory-produced black carbons (biochars). *Environ. Sci. Technol.* **2010**, *44*, 6189–6195.
- (9) Inyang, M.; Gao, B.; Yao, Y.; Xue, Y.; Zimmerman, A. R.; Pullammanappallil, P.; Cao, X. Removal of heavy metals from aqueous solution by biochars derived from anaerobically digested biomass. *Bioresour. Technol.* **2012**, *110*, 50–56.
- (10) Zhang, M.; Gao, B.; Yao, Y.; Xue, Y.; Inyang, M. Synthesis, characterization, and environmental implications of graphene-coated biochar. *Sci. Total Environ.* **2012**, *435–436*, 567–572.
- (11) Xue, Y.; Gao, B.; Yao, Y.; Inyang, M.; Zhang, M.; Zimmerman, A. R.; Ro, K. S. Hydrogen peroxide modification enhances the ability of biochar (hydrochar) produced from hydrothermal carbonization of peanut hull to remove aqueous heavy metals: Batch and column tests. *Chem. Eng. J.* **2012**, *200*, 673–680.
- (12) Beesley, L.; Moreno-Jimenez, E.; Gomez-Eyles, J. L.; Harris, E.; Robinson, B.; Sizmur, T. A review of biochars' potential role in the remediation, revegetation and restoration of contaminated soils. *Environ. Pollut.* **2011**, *159*, 3269–3282.
- (13) Yao, Y.; Gao, B.; Inyang, M.; Zimmerman, A. R.; Cao, X.; Pullammanappallil, P.; Yang, L. Removal of phosphate from aqueous solution by biochar derived from anaerobically digested sugar beet tailings. *J. Hazard. Mater.* **2011**, *190*, 501–507.
- (14) Namasivayam, C.; Sangeetha, D. Equilibrium and kinetic studies of adsorption of phosphate onto ZnCl₂ activated coir pith carbon. *J. Colloid Interface Sci.* **2004**, *280*, 359–365.
- (15) Bhargava, D. S.; Sheldarkar, S. B. Use of Tnsac in phosphate adsorption studies and relationships - Isotherm relationships and utility in the field. *Water Res.* **1993**, *27*, 325–335.
- (16) Yao, Y.; Gao, B.; Zhang, M.; Inyang, M.; Zimmerman, A. R. Effect of biochar amendment on sorption and leaching of nitrate, ammonium, and phosphate in a sandy soil. *Chemosphere* **2012**, *89*, 1467–1471.
- (17) Chen, B. L.; Chen, Z. M.; Lv, S. F. A novel magnetic biochar efficiently sorbs organic pollutants and phosphate. *Bioresour. Technol.* **2011**, *102*, 716–723.
- (18) Yao, Y.; Gao, B.; Inyang, M.; Zimmerman, A. R.; Cao, X.; Pullammanappallil, P.; Yang, L. Biochar derived from anaerobically digested sugar beet tailings: Characterization and phosphate removal potential. *Bioresour. Technol.* **2011**, *102*, 6273–6278.
- (19) Yao, Y.; Gao, B.; Chen, J.; Zhang, M.; Inyang, M.; Li, Y.; Alva, A.; Yang, L. Engineered carbon (biochar) prepared by direct pyrolysis of Mg-accumulated tomato tissues: Characterization and phosphate removal potential. *Bioresour. Technol.* **2013**, *138*, 8–13.
- (20) Zhang, M.; Gao, B.; Yao, Y.; Xue, Y. W.; Inyang, M. Synthesis of porous MgO-biochar nanocomposites for removal of phosphate and nitrate from aqueous solutions. *Chem. Eng. J.* **2012**, *210*, 26–32.
- (21) Zhang, M.; Gao, B.; Varnoosfaderani, S.; Hebard, A. F.; Yao, Y.; Inyang, M. Preparation and characterization of a novel magnetic biochar for arsenic removal. *Bioresour. Technol.* **2013**, *130*, 457–462.
- (22) Zhang, M.; Gao, B.; Yao, Y.; Inyang, M. Phosphate removal ability of biochar/MgAl-LDH ultra-fine composites prepared by liquid-phase deposition. *Chemosphere* **2013**, *92*, 1042–1047.
- (23) Yamada, H.; Kayama, M.; Saito, K.; Hara, M. A fundamental research on phosphate removal by using slag. *Water Res.* **1986**, *20*, 547–557.
- (24) Yan, L. G.; Xu, Y. Y.; Yu, H. Q.; Xin, X. D.; Wei, Q.; Du, B. Adsorption of phosphate from aqueous solution by hydroxy-aluminum, hydroxy-iron and hydroxy-iron-aluminum pillared bentonites. *J. Hazard. Mater.* **2010**, *179*, 244–250.
- (25) Chouyyok, W.; Wiacek, R. J.; Pattamakomsan, K.; Sangvanich, T.; Grudzien, R. M.; Fryxell, G. E.; Yantasee, W. Phosphate removal by anion binding on functionalized nanoporous sorbents. *Environ. Sci. Technol.* **2010**, *44*, 3073–3078.
- (26) Biswas, B. K.; Inoue, K.; Ghimire, K. N.; Ohta, S.; Harada, H.; Ohto, K.; Kawakita, H. The adsorption of phosphate from an aquatic environment using metal-loaded orange waste. *J. Colloid Interface Sci.* **2007**, *312*, 214–223.
- (27) Huang, X.; Liao, X. P.; Shi, B. Adsorption removal of phosphate in industrial wastewater by using metal-loaded skin split waste. *J. Hazard. Mater.* **2009**, *166*, 1261–1265.
- (28) Krishnan, K. A.; Haridas, A. Removal of phosphate from aqueous solutions and sewage using natural and surface modified coir pith. *J. Hazard. Mater.* **2008**, *152*, 527–535.
- (29) Uchimiya, M.; Lima, I. M.; Klasson, K. T.; Wartelle, L. H. Contaminant immobilization and nutrient release by biochar soil amendment: Roles of natural organic matter. *Chemosphere* **2010**, *80*, 935–940.
- (30) Harvey, O. R.; Kuo, L.-J.; Zimmerman, A. R.; Louchouarn, P.; Amonette, J. E.; Herbert, B. E. An index-based approach to assessing recalcitrance and soil carbon sequestration potential of engineered black carbons (biochars). *Environ. Sci. Technol.* **2012**, *46*, 1415–1421.
- (31) Masiello, C.; Druffel, E. Black carbon in deep-sea sediments. *Science* **1998**, *280*, 1911–1913.
- (32) Czimczik, C. I.; Masiello, C. A. Controls on black carbon storage in soils. *Global Biogeochem. Cycles* **2007**, *21*, GB3005.
- (33) Nguyen, B. T.; Lehmann, J.; Kinyangi, J.; Smernik, R.; Riha, S. J.; Engelhard, M. H. Long-term black carbon dynamics in cultivated soil. *Biogeochemistry* **2009**, *92*, 163–176.
- (34) Liang, B.; Lehmann, J.; Solomon, D.; Sohi, S.; Thies, J. E.; Skjemstad, J. O.; Luižā, F. J.; Engelhard, M. H.; Neves, E. G.; Wirick, S. Stability of biomass-derived black carbon in soils. *Geochim. Cosmochim. Acta* **2008**, *72*, 6069–6078.
- (35) Zimmerman, A. R.; Gao, B.; Ahn, M. Y. Positive and negative carbon mineralization priming effects among a variety of biochar-amended soils. *Soil Biol. Biochem.* **2011**, *43*, 1169–1179.
- (36) Zhao, D.; Sengupta, A. K. Ultimate removal of phosphate from wastewater using a new class of polymeric ion exchangers. *Water Res.* **1998**, *32*, 1613–1625.
- (37) Pescod, M. *Wastewater treatment and use in agriculture*; FAO irrigation and drainage paper 47; Food and Agriculture Organization of the United Nations: Rome, 1992.
- (38) Kaneko, S.; Nakajima, K. Phosphorus removal by crystallization using a granular activated magnesia clinker. *J. Water Pollut. Control Fed.* **1988**, *1239–1244*.
- (39) Gakstatter, J. H.; Allum, M. O.; Dominguez, S. E.; Crouse, M. R. A survey of phosphorus and nitrogen levels in treated municipal wastewater. *J. Water Pollut. Control Fed.* **1978**, *718–722*.
- (40) Frimmel, F. H. Aquatic humic substances. *Biopolymers Online*, **2005**: DOI: 10.1002/3527600035.bpol1010.
- (41) Imai, A.; Fukushima, T.; Matsushige, K.; Kim, Y.-H.; Choi, K. Characterization of dissolved organic matter in effluents from wastewater treatment plants. *Water Res.* **2002**, *36*, 859–870.
- (42) Martins, R. C.; Bahia, M. G. A.; Buono, V. T. L. Surface analysis of ProFile instruments by scanning electron microscopy and X-ray energy-dispersive spectroscopy: A preliminary study. *Int. Endod. J.* **2002**, *35*, 848–853.
- (43) Mehlich, A. Mehlich 3 soil test extractant: A modification of Mehlich 2 extractant. *Commun. Soil Sci. Plant Anal.* **1984**, *15*, 1409–1416.
- (44) Axe, L.; Trivedi, P. Intraparticle surface diffusion of metal contaminants and their attenuation in microporous amorphous Al, Fe, and Mn oxides. *J. Colloid Interface Sci.* **2002**, *247*, 259–265.
- (45) Weerasooriya, R.; Tobschall, H. J.; Seneviratne, W.; Bandara, A. Transition state kinetics of Hg (II) adsorption at gibbsite-water interface. *J. Hazard. Mater.* **2007**, *147*, 971–978.
- (46) Gerente, C.; Lee, V. K. C.; Le Cloirec, P.; McKay, G. Application of chitosan for the removal of metals from wastewaters by adsorption - Mechanisms and models review. *Crit. Rev. Environ. Sci. Technol.* **2007**, *37*, 41–127.
- (47) Fournier, V.; Marcus, P.; Olefjord, I. Oxidation of magnesium. *Surf. Interface Anal.* **2002**, *34*, 494–497.
- (48) Song, Y.; Shan, D.; Chen, R.; Zhang, F.; Han, E. H. Formation mechanism of phosphate conversion film on Mg-8.8 Li alloy. *Corros. Sci.* **2009**, *51*, 62–69.

- (49) Lv, J.; Qiu, L.; Qu, B. Controlled growth of three morphological structures of magnesium hydroxide nanoparticles by wet precipitation method. *J. Cryst. Growth* **2004**, *267*, 676–684.
- (50) Henrist, C.; Mathieu, J. P.; Vogels, C.; Rulmont, A.; Cloots, R. Morphological study of magnesium hydroxide nanoparticles precipitated in dilute aqueous solution. *J. Cryst. Growth* **2003**, *249*, 321–330.
- (51) Zhang, W.; Tian, B.; Du, K. Q.; Zhang, H. X.; Wang, F. H. Preparation and corrosion performance of PEO coating with low porosity on magnesium alloy AZ91D in acidic KF system. *Int. J. Electrochem. Sci.* **2011**, *6*, 5228–5248.
- (52) Song, Y.; Shan, D.; Chen, R.; Zhang, F.; Han, E. H. A novel phosphate conversion film on Mg-8.8 Li alloy. *Surf. Coat. Technol.* **2009**, *203*, 1107–1113.
- (53) Chusuei, C.; Goodman, D.; Van Stipdonk, M.; Justes, D.; Loh, K.; Schweikert, E. Solid-liquid adsorption of calcium phosphate on TiO_2 . *Langmuir* **1999**, *15*, 7355–7360.
- (54) Vanderkooi, G. Crystal-refined hydrogen-bond potentials for interactions involving the phosphate group. *J. Phys. Chem.* **1983**, *87*, 5121–5129.
- (55) Burget, U.; Zundel, G. Glutamic acid-dihydrogen phosphate hydrogen-bonded networks: Their proton polarizability as a function of cations present. Infrared investigations. *Biophys. J.* **1987**, *52*, 1065–1070.
- (56) Pierzynski, G. M. *Methods of phosphorus analysis for soils, sediments, residuals, and waters*. North Carolina State University: Raleigh, NC, 2000.
- (57) Gaskin, J.; Steiner, C.; Harris, K.; Das, K.; Bibens, B. Effect of low-temperature pyrolysis conditions on biochar for agricultural use. *Trans. ASABE* **2008**, *51*, 2061–2069.
- (58) Solaiman, Z. M.; Murphy, D. V.; Abbott, L. K. Biochars influence seed germination and early growth of seedlings. *Plant Soil* **2012**, *1*–15.
- (59) Austin, R. The growth of watercress (*Rorippa nasturtium aquaticum* (L.) Hayek) from seed as affected by the phosphorus nutrition of the parent plant. *Plant Soil* **1966**, *24*, 113–120.